Applied Physics A (2025) 131:123
https://doi.org/10.1007/s00339-025-08245-z

Applied Physics A
Materials Science & Processing

A study on radiation interaction parameters of boron carbide/zirconium boride composites

M. F. Turhan[1] · A. Tursucu[2] · H. Oğul[3] · M. R. Kaçal[4] · H. Polat[5] · E. Colak[6] · S. Yurtcan[7] · F. Akman[8]

Received: 10 September 2024 / Accepted: 6 January 2025 / Published online: 21 January 2025

Abstract

In this study, photon interaction parameters such as radiation protection efficiency (*RPE*), total mass attenuation coefficient (μ/ρ), linear attenuation coefficients (μ), half value layers (*HVL*), tenth value layers (*TVL*), mean free paths (*MFP*), effective atomic numbers (Z_{Eff}) and effective electron densities (N_{Eff}) were experimentally investigated for the BCZrB-0, BCZrB-10, BCZrB-20, BCZrB-30, BCZrB-40 and BCZrB-50 in the energy range from 59.5 keV to 1332.5 keV. In the experiment, HPGe detector and ^{241}Am (59.5 keV), ^{133}Ba (81 keV, 276.4 keV, 302.9 keV, 356 keV and 383.9 keV), ^{22}Na (511 keV and 1274.5 keV), ^{137}Cs (661.7 keV), and ^{60}Co (1173.2 keV and 1332.5 keV) radioactive point sources were used. Experimental results compared with results of the WinXCOM, GEANT4 simulation code and FLUKA simulation code. Energy absorption build-up factors (*EABF*) and exposure build-up factors (*EBF*) were calculated with G-P fitting method in the energy region 0.015 MeV ≤ E ≤ 15 MeV. Kerma relative to air values were investigated in the energy region 0.001 MeV ≤ E ≤ 20 MeV. Effective removal cross section, total macroscopic cross section and number of transmitted neutron values were defined for composites. The agreement between experimental and WinXCOM program, between experimental and GEANT 4 simulation codes and between experimental and FLUKA simulation codes of gamma-ray interaction parameters are < 5.1%, < 6.5% and < 5%, respectively. All of the results are compatible with each other and BCZrB-50 is a good gamma-ray radiation absorber in the studied composites and BCZrB-0 is the best neutron absorber in the studied composites.

Keywords Attenuation coefficient · Effective atomic number · Kerma relative to air · Gamma-ray buildup factor · Cross section

1 Introduction

Today, radiation is used in many fields such as radiotherapy, nuclear medicine, radiology for the purpose of diagnosis and treatment in medicine, physics, agriculture, geology and many others for the benefit of humanity [1–5]. Although ionizing radiation has used in many application areas for humanity, it is obvious that it has harmful effects on human health. Considering these harmful effects, various radiation shielding materials are produced today to protect against

✉ M. F. Turhan
m.f.turhan@hotmail.com

1 Atatürk Vocational School of Health Service, Department of Medical Imaging Techniques, Afyonkarahisar Health Sciences University, 03200 Afyonkarahisar, Turkey

2 Engineering Faculty, Department of Electrical and Electronics Engineering, Şırnak University, 73000 Sirnak, Turkey

3 Faculty of Engineering and Architecture, Department of Nuclear Engineering, Sinop University, 57000 Sinop, Turkey

4 Arts and Sciences Faculty, Department of Physics, Giresun University, 28100 Giresun, Turkey

5 Vocational School of Technical Sciences, Department of Architecture and Urban Planning, Bingöl University, 12000 Bingöl, Turkey

6 Department of Energy System Engineering, Giresun University, Engineering Faculty, 28100 Giresun, Turkey

7 Central Research Laboratory Application and Research Center, Giresun University, 28100 Giresun, Turkey

8 Vocational School of Social Sciences, Department of Property Protection and Security, Bingöl University, Program of Occupational Health and Safety, 12000 Bingöl, Turkey

ionizing radiation, and the interactions of these materials with radiation are examined. Some of these studies are carried out on the radiation attenuation parameters of composites [3, 6–20]. Composite materials have many advantages such as excellent resistance, high strength-to-weight ratio, long-lived, easy to produce, lover cost, lightweight, etc. Because of these advantages, it is used in many fields such as medicine, aerospace, construction industry, automotive industry, chemical industry, etc. Radiation transmission factors (*TF*), mass attenuation coefficients (μ/ρ), linear attenuation coefficients (μ), half value layers (*HVL*), mean free paths (*MFP*), effective atomic numbers (Z_{eff}), effective electron densities (N_{eff}), equivalent atomic numbers (Z_{eq}), energy absorption build-up factors (*EABF*) and exposure build-up factors (*EBF*) for hematite doped polymer composites were determined by Turhan et al. [6]. μ/ρ, Z_{Eff}, N_{eff}, *HVL*, *TVL* and *MFP* were determined both experimentally and computationally in the gamma photon energies ranging from 303 to 1332 keV for polycarbonate loaded with different filler of bismuth nitrate pentahydrate ($Bi(NO_3)_3{\cdot}5H_2O$ or BNP) by Mirji and Lobo [9]. Dong et al. [15] evaluated gamma-ray attenuation parameters and mechanism of boron rich slag/epoxy resin shielding composites. Akman et al. [3] determined the μ/ρ, μ, *HVL*, tenth-value layer (*TVL*), *MFP*, Z_{Eff} and N_{Eff} values for niobium-reinforced novel polymer composite in the energy region 59.5 keV ≤ E ≤ 1408 keV.

In this study, BCZrB-0, BCZrB-10, BCZrB-20, BCZrB-30, BCZrB-40 and BCZrB-50 composite materials were prepared to investigate the gamma and neutron interaction parameters. While preparing the composites, boron carbide (B_4C) and zirconium boride (ZrB_2) compounds were used. Boron carbide is one of the hardest materials [21]. Because of this feature, it is extensively used in industry as an abrasive for polishing, for cutting applications including water jet cutting. It is also used in nuclear power plants because of good absorbent for neutrons and in many fields such as military industry, construction industry, etc. [22]. Zirconium boride that is the other compound used to form the composite has low density, high hardness, good high temperature strength and anticorrosion ability, high thermal and electrical conductivity, and excellent thermal shock resistance, etc. [23]. ZrB_2 is used as basis material in many technological applications such as aerospace, furnace elements, electrodes, nuclear industry and etc. [24, 25].

In the study, radiation protection efficiency (*RPE*), μ/ρ, μ, *HVL*, *TVL*, *MFP*, Z_{eff} and N_{eff} for the BCZrB-0, BCZrB-10, BCZrB-20, BCZrB-30, BCZrB-40 and BCZrB-50 in the energy range from 59.5 keV to 1332.5 keV were experimentally determined. Measurements were taken at 11 different energy in the energy region 59.5 keV ≤ E ≤ 1332.5 keV, which is used especially in medical applications as brachytherapy, tomography, radiotherapy, nuclear medicine and many others. The aim of this study is to compare the experimental radiation interaction parameters of boron carbide/zirconium boride composites with WinXCOM, GEANT4 simulation code and FLUKA simulation code. Both the agreement of experimental results with WinXCOM and GEANT4 simulation code and FLUKA simulation code results and the agreement between GEANT4 simulation code results and FLUKA simulation code results were demonstrated for the BCZrB-0, BCZrB-10, BCZrB-20, BCZrB-30, BCZrB-40 and BCZrB-50. Secondly, *EABF* and *EBF* for BCZr composites in the energy region 0.015 MeV ≤ E ≤ 15 MeV were evaluated with G-P fitting method. Also, kerma relative to air parameters were calculated in the energy range from 0.001 MeV to 20 MeV for ternary composites. Finally, theoretically calculated effective removal cross section, total macroscopic cross section from GEANT4, mean free path determined from GEANT4 and number of transmitted neutron values from GEANT4 were determined for BCZrB-0, BCZrB-10, BCZrB-20, BCZrB-30, BCZrB-40 and BCZrB-50. To the best of our knowledge, parameters given in the study for BCZrB-0, BCZrB-10, BCZrB-20, BCZrB-30, BCZrB-40 and BCZrB-50 have been comprehensively determined for the first time in this study.

2 Experimental procedure

2.1 Polymer composite manufacturing process

In the conducted study, polymer composites were produced using unsaturated polyester resin, MEKP, cobalt, and boron carbide (B_4C) or Zirconium boride (ZrB_2) as filler materials. Six groups of samples, including a control group, were produced. The control sample was produced as a composite material made of 50% unsaturated polyester resin and 50% boron carbide as filler material. This sample was codded as BCZrB-0. MEKP (methyl ethyl ketone and peroxide) was used to initiate the polymerization reaction, followed by the addition of cobalt octoate (6%) in appropriate amounts to accelerate the reaction. In the second stage, zirconium boride was substituted for boron carbide at volumetric ratios of 10%, 20%, 30%, 40%, and 50% to produce the other group samples. The coding of the samples was done according to the ratio of zirconium boride in the sample. For example, the sample containing 50% unsaturated polyester resin, 30% boron carbide and 20% zirconium boride was codded as BCZrB-20. If the sample contained 50% unsaturated polyester resin, 10% boron carbide and 40% zirconium boride, this sample was coded BCZrB-40. The produced composites are cylindrical in shape and have a diameter of 20 mm and a thickness of 10 mm.

The density of the sample was evaluated with Archimedes principle as follow [26];

$$\rho = \left[\frac{A}{A-B}\right]\rho_w \quad (1)$$

where A, B, ρ_w are sample weight in air, sample weight in water and density of water, respectively.

2.2 Sample analysis process

The strategy of this research relies on the gamma-ray shielding investigation of the considered samples using experiment, MC simulations and theoretical calculations. The used experimental apparatus consists of the HPGe detector, collimators, point sources, preamplifier, amplifier and Multi-Channel Analyzer (MCA) as illustrated in Fig. 1. HPGe detector (ORTEC, GEM-SP7025P4-B model), whose values are determined by the manufacturer company (ORTEC), has 70 mm active crystal diameter, 25 mm crystal width and 380 eV, 585 eV and 1.8 keV at 5.9 keV, 122 keV and 1.33 MeV resolutions, respectively. To collimate the radiation beam, lead blocks with a thickness of 5 cm and a span of 3 cm (first collimator according to source) and 2 cm (second collimator according to source) were used as shown in Fig. 1. The detector was shielded by a collimator made of Pb (4.2 mm), Fe (1.1 mm) and Al (1.0 mm) in order to reduce background noise. The sample is located between the point gamma-ray source and the HPGe detector. Here, in order to obtain the desired gamma-ray energies, the following radiation point sources have been used: ^{241}Am (59.5 keV), ^{133}Ba (81 keV, 276.4 keV, 302.9 keV, 356 keV and 383.9 keV), ^{22}Na (511 keV and 1274.5 keV), ^{137}Cs (661.7 keV), and ^{60}Co (1173.2 keV and 1332.5 keV). In order to have sufficient (minimum 1xE^4 count under the related peak) statistical uncertainty, the measurement period was carried out as 1200 s for each radioactive source. For each point source, the gamma-ray peaks and their corresponding net area of the peak were obtained three times to safely evaluate the statistical uncertainties for each sample. Measurements were repeated three times for each sample.

Theoretical calculations and Monte Carlo simulations were performed to complement the experimental characterization of the proposed shielding materials.

The mass attenuation coefficients of the considered materials were calculated with WinXCOM [27] and compared to experimental results using HPGe detector. MC

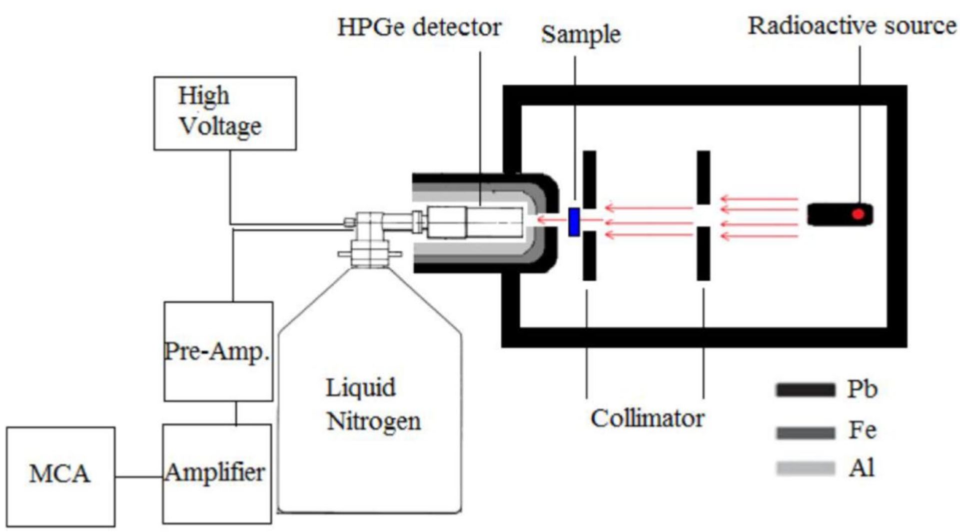

Fig. 1 The experimental arrangement

Table 1 Chemical content and densities of composites containing B_4C, ZrB_2 and polyester

Volume %			Sample Code	Percent elemental composition						ρ (g/cm³) Exper	ρ (g/cm³) Theor
Polyester resin	B_4C	ZrB_2		H	B	C	O	Co	Zr		
50	50	–	BCZrB-0	1.3917	53.9828	33.6818	10.9401	0.0037	–	1.7508	1.8160
50	40	10	BCZrB-10	1.3917	49.9061	32.1824	10.9401	0.0037	5.5760	1.7666	1.8705
50	30	20	BCZrB-20	1.3917	45.8295	30.6831	10.9401	0.0037	11.1520	1.8373	1.9283
50	20	30	BCZrB-30	1.3917	41.7528	29.1838	10.9401	0.0037	16.7280	1.9213	1.9897
50	10	40	BCZrB-40	1.3917	37.6762	27.6844	10.9401	0.0037	22.3039	2.0400	2.0553
50	–	50	BCZrB-50	1.3917	33.5995	26.1851	10.9401	0.0037	27.8799	2.0781	2.1253

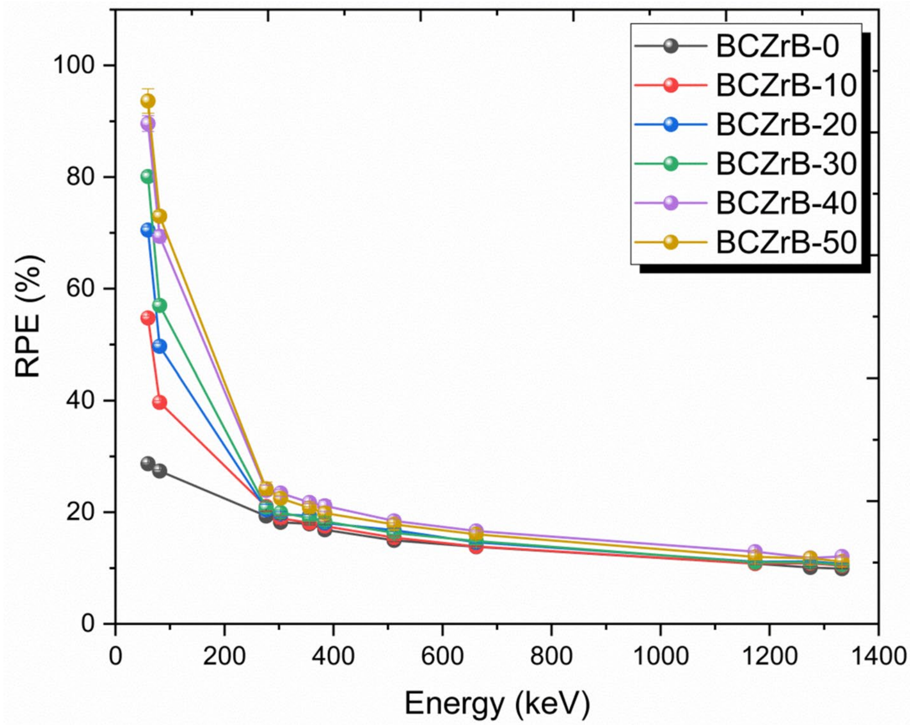

Fig. 2 *RPE* values of the ternary composites versus photon energy

simulations are another technique to calculate the mass attenuation coefficients of any considered material. The chosen simulation packages were GEANT4 [28] and FLUKA [29] since recent reports on radiation shielding studies showed that both packages provide results in remarkable agreement with experimental outcomes [30–33]. Another motivation to choose these simulation packages are the fact that they are publicly available software tools commonly used in radiation related studies. In both simulation packages, the chosen materials are modelled by defining their thickness, elemental weights, densities. Then, $1xE^7$ gamma particles were fired onto the modelled material with a monochromatic energy. The chosen gamma energies are identical to the energies of the gamma-rays emitted by the investigated radioactive sources. Using the number of transmitted photons obtained from simulation programs, user could easily calculate the gamma-ray shielding parameters such as μ/ρ, μ, *HVL*, *MFP*, Z_{Eff} and many others.

The neutron shielding effectiveness for the absorbers under study was evaluated in the second part of the study. In this case, unfortunately we could not perform any experimental characterization. Therefore, effective neutron removal cross sections for the composites under investigation are theoretically determined with GEANT4.

3 Data analysis procedure

3.1 Calculation of *RPE*, *μ/ρ*, *μ*, *HVL*, *TVL* and *MFP*

Radiation protection efficiency (*RPE*) is essential in estimating the number of gamma or X-ray photons blocked by absorber samples and given as [3];

$$RPE(\%) = \left(1 - \frac{I}{I_o}\right)x100 \tag{2}$$

where, I_o and I values represent incident photons intensity and the transmitted photon intensity on the target absorber, respectively.

The total mass absorption coefficient (μ/ρ), which is of great importance in radiation shielding calculations, is computed as follow [12];

$$\frac{\mu}{\rho} = -\frac{1}{\rho x} ln\left(\frac{I}{I_0}\right) \tag{3}$$

where, ρ and x are the density and thickness of the target, respectively. The mass attenuation coefficient for a composite is determined by [6];

$$(\mu/\rho)_{comp.} = \sum_i w_i(\mu/\rho)_i \tag{4}$$

Table 2 The experimental, theoretical and simulations results of the μ/ρ ($cm^2\ g^{-1}$) for the ternary composites

Energy (keV)	BCZrB-0				BCZrB-10				BCZrB-20			
	Exp	WinX	GEANT4	FLUKA	Exp	WinX	GEANT4	FLUKA	Exp	WinX	GEANT4	FLUKA
59.5	0.1700 ± 0.0035	0.1704	0.1622	0.1707	0.3793 ± 0.0080	0.3749	0.3550	0.3749	0.5697 ± 0.0122	0.5794	0.5472	0.5791
81.0	0.1608 ± 0.0036	0.1559	0.1505	0.1559	0.2418 ± 0.0052	0.2403	0.2292	0.2406	0.3204 ± 0.0073	0.3248	0.3176	0.3244
276.4	0.1080 ± 0.0048	0.1070	0.1062	0.1070	0.1131 ± 0.0052	0.1093	0.1079	0.1092	0.1070 ± 0.0053	0.1115	0.1096	0.1115
302.9	0.1011 ± 0.0035	0.1034	0.1028	0.1034	0.1003 ± 0.0031	0.1051	0.1040	0.1051	0.1020 ± 0.0033	0.1068	0.1052	0.1068
356.0	0.0993 ± 0.0022	0.0973	0.0970	0.0976	0.0955 ± 0.0021	0.0983	0.0973	0.0983	0.1005 ± 0.0023	0.0993	0.0984	0.0992
383.9	0.0930 ± 0.0051	0.0945	0.0946	0.0948	0.0921 ± 0.0047	0.0952	0.0947	0.0952	0.0930 ± 0.0045	0.0960	0.0949	0.0959
511.0	0.0816 ± 0.0021	0.0841	0.0840	0.0840	0.0804 ± 0.0021	0.0843	0.0843	0.0838	0.0859 ± 0.0023	0.0845	0.0844	0.0841
661.7	0.0747 ± 0.0016	0.0751	0.0757	0.0749	0.0715 ± 0.0016	0.0751	0.0755	0.0751	0.0738 ± 0.0016	0.0752	0.0754	0.0749
1173.2	0.0575 ± 0.0013	0.0573	0.0571	0.0570	0.0549 ± 0.0013	0.0572	0.0570	0.0567	0.0551 ± 0.0013	0.0571	0.0568	0.0565
1274.5	0.0536 ± 0.0014	0.0547	0.0555	0.0547	0.0550 ± 0.0014	0.0546	0.0551	0.0548	0.0555 ± 0.0014	0.0545	0.0547	0.0545
1332.5	0.0524 ± 0.0012	0.0537	0.0538	0.0535	0.0527 ± 0.0012	0.0535	0.0535	0.0533	0.0532 ± 0.0012	0.0534	0.0534	0.0531
Energy (keV)	BCZrB-30				BCZrB-40				BCZrB-50			
	Exp	WinX	GEANT4	FLUKA	Exp	WinX	GEANT4	FLUKA	Exp	WinX	GEANT4	FLUKA
59.5	0.7573 ± 0.0169	0.7838	0.7421	0.7838	0.9484 ± 0.0240	0.9883	0.9334	0.9895	1.1770 ± 0.0362	1.1928	1.1262	1.1941
81.0	0.3959 ± 0.0094	0.4093	0.3959	0.4094	0.4961 ± 0.0126	0.4937	0.4733	0.4940	0.5597 ± 0.0130	0.5782	0.5515	0.5781
276.4	0.1097 ± 0.0052	0.1138	0.1111	0.1138	0.1146 ± 0.0051	0.1160	0.1129	0.1160	0.1187 ± 0.0063	0.1183	0.1148	0.1183
302.9	0.1045 ± 0.0032	0.1084	0.1065	0.1084	0.1120 ± 0.0037	0.1101	0.1076	0.1101	0.1091 ± 0.0033	0.1118	0.1086	0.1118
356.0	0.0986 ± 0.0022	0.1002	0.0990	0.1003	0.1029 ± 0.0023	0.1012	0.0995	0.1016	0.0997 ± 0.0023	0.1022	0.1001	0.1027
383.9	0.0952 ± 0.0047	0.0967	0.0958	0.0967	0.0997 ± 0.0051	0.0975	0.0961	0.0978	0.0947 ± 0.0056	0.0982	0.0965	0.0986
511.0	0.0836 ± 0.0022	0.0848	0.0844	0.0846	0.0856 ± 0.0022	0.0850	0.0846	0.0847	0.0841 ± 0.0021	0.0852	0.0846	0.0851
661.7	0.0754 ± 0.0016	0.0752	0.0754	0.0750	0.0764 ± 0.0017	0.0752	0.0751	0.0750	0.0749 ± 0.0016	0.0752	0.0752	0.0748
1173.2	0.0550 ± 0.0013	0.0569	0.0571	0.0565	0.0581 ± 0.0013	0.0568	0.0568	0.0565	0.0548 ± 0.0013	0.0567	0.0565	0.0562
1274.5	0.0550 ± 0.0014	0.0543	0.0544	0.0541	0.0528 ± 0.0014	0.0542	0.0545	0.0541	0.0535 ± 0.0014	0.0541	0.0544	0.0541
1332.5	0.0525 ± 0.0012	0.0533	0.0535	0.0529	0.0540 ± 0.0012	0.0532	0.0531	0.0530	0.0507 ± 0.0011	0.0530	0.0530	0.0526

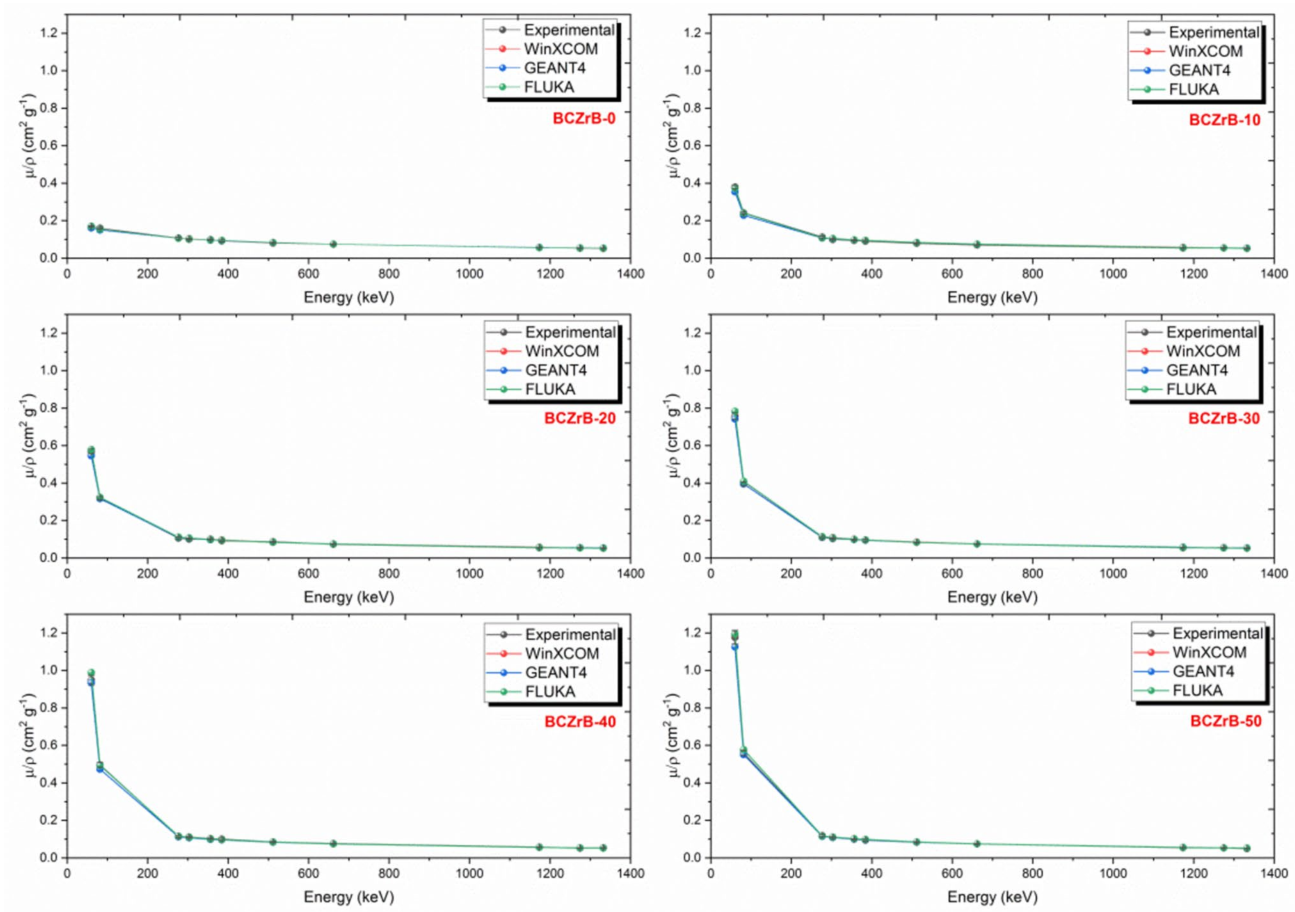

Fig. 3 Total mass attenuation coefficients of the ternary composites versus photon energy

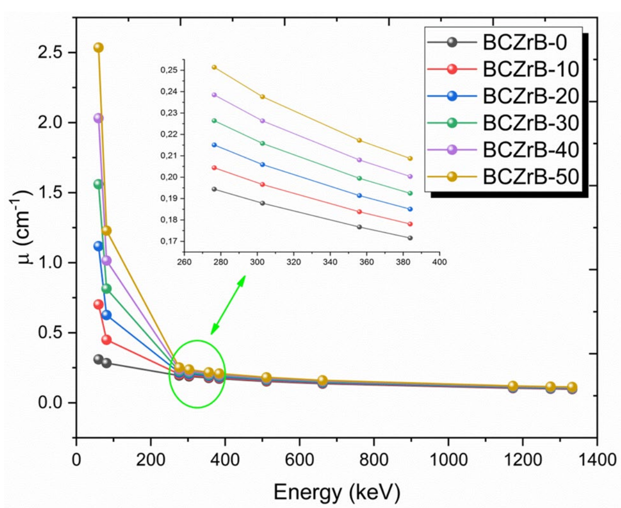

Fig. 4 Linear attenuation coefficients of the ternary composites versus photon energy

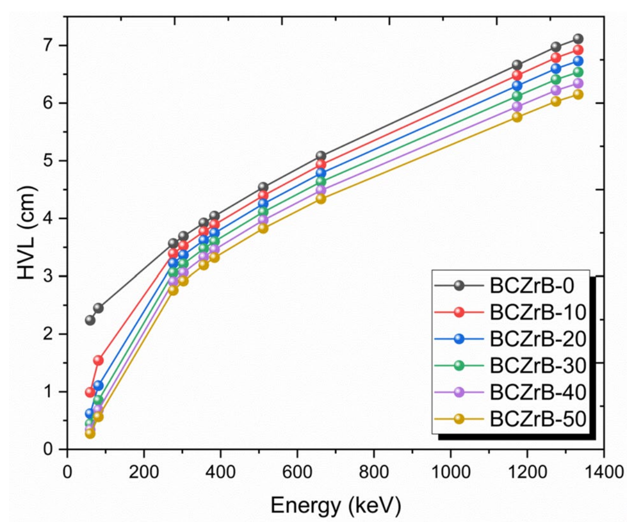

Fig. 5 *HVL* values of the ternary composites versus photon energy

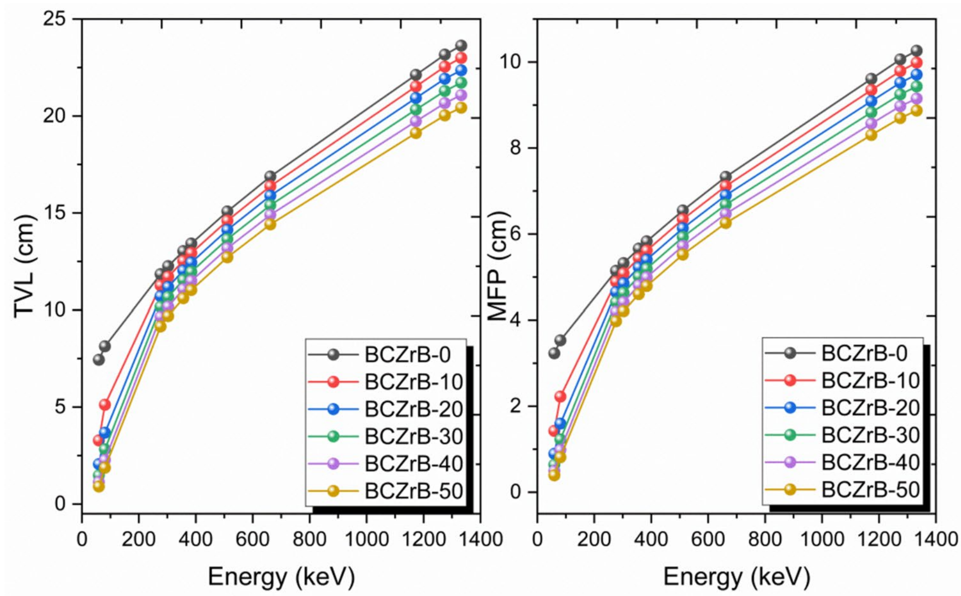

Fig. 6 *TVL* and *MFP* values of the ternary composites versus photon energy

$$w_i = \frac{n_i A_i}{\sum_j n_j A_j} \quad (5)$$

here, *w,* $(\mu/\rho)_i$, n_i and A_i are the weight fraction, the mass attenuation coefficient of the ith constituent element in the compound, number of atoms of ith constituent element in the compound and the atomic weight of the ith element in the compound, respectively. Let be an example for experimental calculation procedure of μ/ρ at 81 keV for BCZrB-10 ternary composite. Here, I_o is 43.52 cps (count per second), I as transmitted photon intensity on the BCZrB-10 is 26.25 cps and ρx is 2.09 g/cm^2. Then, using these values in Eq. (3), the μ/ρ for BCZrB-10 at 81 keV is experimentally determined as 0.2418 cm^2/g.

μ can be computed with μ/ρ and density (ρ). Table 1 shows the chemical content and densities of BCZrB-0, BCZrB-10, BCZrB-20, BCZrB-30, BCZrB-40 and BCZrB-50.

The half-value layer (*HVL*) and the tenth-value layer (*TVL*) have been determined with Eq. 6 and 7, respectively [7, 12].

$$HVL = \frac{\ln 2}{\mu} \quad (6)$$

$$TVL = \frac{\ln 10}{\mu} \quad (7)$$

The mean free path (*MFP*) has been evaluated with the Eq. 8 [6].

$$MFP = \frac{1}{\mu} \quad (8)$$

In the Eq. 8, μ is linear attenuation coefficient.

3.2 Calculation of Z_{eff} and N_{eff}

Z_{eff} and N_{eff} are determined as follow [8];

$$Z_{eff} = \frac{\sum_i f_i A_i (\mu/\rho)_i}{\sum_j f_j \frac{A_j}{Z_j} (\mu/\rho)_j} \quad (9)$$

$$N_{eff} = \frac{Z_{eff}}{A_{tot}} \left(N n_{tot} \right) \quad (10)$$

where, the fractional abundance of the constituent element in the compound is symbolized with *fi*. *Ai* and *Zj* characterize the atomic weight and atomic number of the constituent element in the compound, respectively. Total atomic weight of compound, total number of atoms and Avogadro constant are indicated as A_{tot}, n_{tot} and *N*, respectively.

3.3 Calculation of energy absorption and exposure buildup factors.

Photon buildup factor calculations consist of three parts; calculation of the material's equivalent atomic number (Z_{eq}), analysis of geometric sequence (G-P) fitting parameters, and estimation of energy absorption buildup factor (*EABF*) and exposure buildup factor (*EBF*) parameters.

In order to calculate Z_{eq}, Compton partial mass attenuation coefficient ($(\mu/\rho)_{Compton}$) and total mass attenuation coefficient ($(\mu/\rho)_{Total}$) were calculated using WinXCOM [27] for both the elements in the atomic number range from 4 to 36 and composites in the energy 0.015 MeV ≤ E ≤ 15 MeV. After $(\mu/\rho)_{Compton}$ and $(\mu/\rho)_{Total}$ were calculated, $(\mu/\rho)_{Compton}/(\mu/\rho)_{Total}$ values were determined both elements

Table 3 The experimental, theoretical and simulations results of the Z_{eff} for the ternary composites

Energy (keV)	BCZrB-0				BCZrB-10				BCZrB-20			
	Exp	Theo	GEANT4	FLUKA	Exp	Theo	GEANT4	FLUKA	Exp	Theo	GEANT4	FLUKA
59.5	4.978 ± 0.103	4.990	4.748	4.998	10.046 ± 0.211	9.931	9.403	9.930	13.777 ± 0.295	14.012	13.234	14.004
81.0	5.118 ± 0.113	4.960	4.789	4.960	7.521 ± 0.162	7.476	7.128	7.483	9.746 ± 0.222	9.881	9.662	9.869
276.4	4.983 ± 0.220	4.936	4.895	4.934	5.441 ± 0.248	5.259	5.194	5.255	5.380 ± 0.266	5.611	5.516	5.609
302.9	4.825 ± 0.165	4.935	4.904	4.933	4.999 ± 0.155	5.236	5.183	5.236	5.314 ± 0.172	5.565	5.485	5.565
356.0	5.037 ± 0.113	4.934	4.921	4.949	5.061 ± 0.113	5.208	5.156	5.209	5.575 ± 0.126	5.507	5.458	5.502
383.9	4.856 ± 0.266	4.935	4.941	4.950	5.028 ± 0.257	5.199	5.171	5.197	5.319 ± 0.259	5.488	5.425	5.482
511.0	4.788 ± 0.125	4.934	4.931	4.929	4.937 ± 0.129	5.175	5.174	5.145	5.526 ± 0.147	5.438	5.432	5.410
661.7	4.903 ± 0.106	4.933	4.973	4.918	4.913 ± 0.107	5.162	5.188	5.158	5.317 ± 0.116	5.413	5.432	5.396
1173.2	4.953 ± 0.114	4.937	4.919	4.907	4.951 ± 0.114	5.155	5.139	5.113	5.209 ± 0.120	5.395	5.375	5.339
1274.5	4.816 ± 0.124	4.922	4.989	4.916	5.173 ± 0.134	5.139	5.183	5.154	5.480 ± 0.141	5.377	5.402	5.382
1332.5	4.826 ± 0.108	4.940	4.949	4.929	5.075 ± 0.113	5.158	5.159	5.132	5.377 ± 0.120	5.398	5.400	5.371
Energy (keV)	BCZrB-30				BCZrB-40				BCZrB-50			
	Exp	Theo	GEANT4	FLUKA	Exp	Theo	GEANT4	FLUKA	Exp	Theo	GEANT4	FLUKA
59.5	16.849 ± 0.376	17.440	16.510	17.439	19.537 ± 0.495	20.360	19.228	20.385	22.575 ± 0.695	22.877	21.600	22.903
81.0	11.784 ± 0.279	12.182	11.783	12.184	14.456 ± 0.366	14.386	13.790	14.395	15.970 ± 0.371	16.500	15.737	16.496
276.4	5.783 ± 0.274	5.996	5.857	5.995	6.339 ± 0.280	6.420	6.248	6.417	6.910 ± 0.365	6.888	6.683	6.890
302.9	5.708 ± 0.177	5.926	5.816	5.924	6.430 ± 0.214	6.323	6.176	6.321	6.598 ± 0.201	6.763	6.567	6.762
356.0	5.743 ± 0.128	5.836	5.763	5.839	6.303 ± 0.142	6.198	6.096	6.219	6.440 ± 0.146	6.601	6.462	6.634
383.9	5.715 ± 0.285	5.805	5.748	5.805	6.295 ± 0.322	6.156	6.069	6.180	6.311 ± 0.372	6.546	6.434	6.573
511.0	5.648 ± 0.147	5.729	5.707	5.717	6.092 ± 0.160	6.050	6.019	6.033	6.320 ± 0.161	6.407	6.361	6.400
661.7	5.710 ± 0.125	5.689	5.705	5.679	6.091 ± 0.132	5.996	5.992	5.982	6.309 ± 0.137	6.337	6.340	6.305
1173.2	5.470 ± 0.127	5.659	5.672	5.621	6.088 ± 0.141	5.951	5.951	5.915	6.070 ± 0.141	6.277	6.262	6.224
1274.5	5.703 ± 0.148	5.640	5.650	5.613	5.774 ± 0.149	5.931	5.960	5.913	6.193 ± 0.159	6.256	6.294	6.251
1332.5	5.578 ± 0.124	5.662	5.684	5.624	6.048 ± 0.134	5.955	5.946	5.938	6.003 ± 0.134	6.281	6.272	6.230

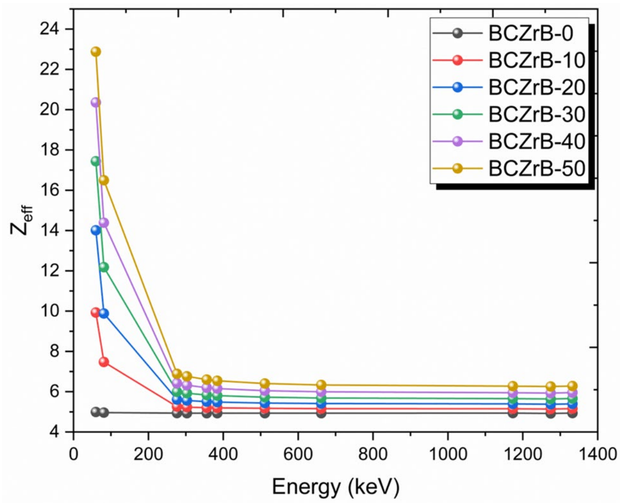

Fig. 7 Z_{Eff} values of the ternary composites versus photon energy

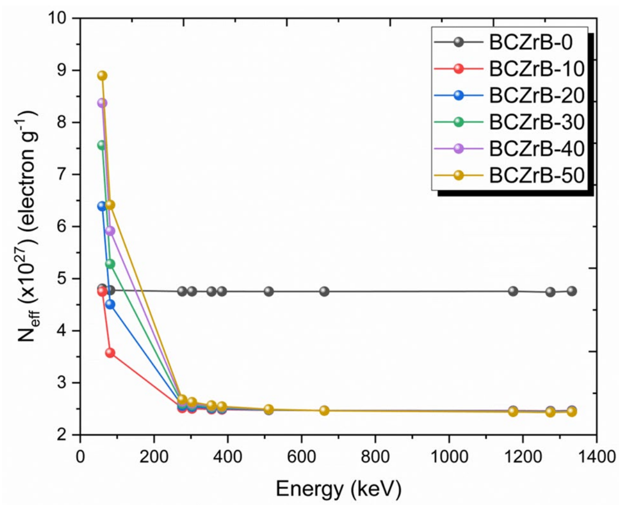

Fig. 8 N_{Eff} values of the ternary composites versus photon energy

and composites. Z_{eq} is computed by matching $(\mu/\rho)_{Compton}/(\mu/\rho)_{Total}$ of the specific energy for both elements and composites. When the $(\mu/\rho)_{Compton}/(\mu/\rho)_{Total}$ value of the composite lies among two consecutive ratios $(\mu/\rho)_{Compton}$ to $(\mu/\rho)_{Total}$ of elements, the interpolation of the Z_{eq} of a composite is calculated as follow [6, 34];

$$Z_{eq} = \frac{Z_1\left(\log R_2 - \log R\right) + Z_2\left(\log R - \log R_1\right)}{\log R_2 - \log R_1} \tag{11}$$

where, R_1, R_2 and R are the $(\mu/\rho)_{Compton}/(\mu/\rho)_{Total}$ for the two consecutive elements and composite at specific energy, respectively. Z_1 and Z_2 are the atomic numbers of the corresponding elements.

Geometric progression (G-P) fitting parameters for a composite are interpolated similar to Z_{eq} as follow;

$$P = \frac{P_1\left(\log Z_2 - \log Z_{eq}\right) + P_2\left(\log Z_{eq} - \log Z_1\right)}{\log Z_2 - \log Z_1} \tag{12}$$

P_1 and P_2 are the G-P fitting parameters (b, c, a, X_k and d) of the corresponding elements at a given energy. The G-P fitting coefficients for elements were taken from the ANSI/ANS-6.4.3 [35] standard reference database.

EABF and *EBF* are determined as follow;

$$B(E,x) = 1 + \frac{b-1}{b+1}(K^x - 1) \quad \text{for } K \neq 1 \tag{13}$$

$$B(E,x) = 1 + (b-1)x \quad \text{for} \quad K = 1 \tag{14}$$

in these equations, K represents as following;

$$K(E,x) = cx^a + d\frac{\tanh(x/X_k - 2) - \tanh(-2)}{1 - \tanh(-2)} \quad \text{for} \quad x \leq 40mfp \tag{15}$$

where, a, b, c, d, and X_k are G-P fitting parameters and b is the value of buildup factor at 1 mfp. E represents the energy of the incident photon. x is the mean free path (mfp).

3.4 Calculation of kerma relative to air and effective removal cross-section

The kerma relative to air can be calculated with Eq. 16 [34].

$$Kermarelativetoair = \frac{\left(\mu_{en}/\rho\right)_{Comp.}}{\left(\mu_{en}/\rho\right)_{Air}} \tag{16}$$

$$\left(\frac{\mu_{en}}{\rho}\right)_{Comp.} = \sum w_i \left(\frac{\mu_{en}}{\rho}\right)_i \tag{17}$$

$$w_i = \frac{n_i A_i}{\sum_j n_j A_j} \tag{18}$$

here, w_i and $(\mu_{en}/\rho)_i$ are the weight fraction and the mass energy absorption coefficient of the ith constituent element, respectively. n_i and A_i are number of atoms of the ith constituent element in the compound and the atomic weight of the ith element in the compound, respectively.

Effective removal cross sections for mixtures, alloys, and compounds can be calculated by knowing the partial density and mass removal cross section as follow [36, 37];

$$\Sigma_R = \sum_i W_i\left(\Sigma_R/\rho\right)_i \tag{19}$$

in this equation, W_i represents as follow;

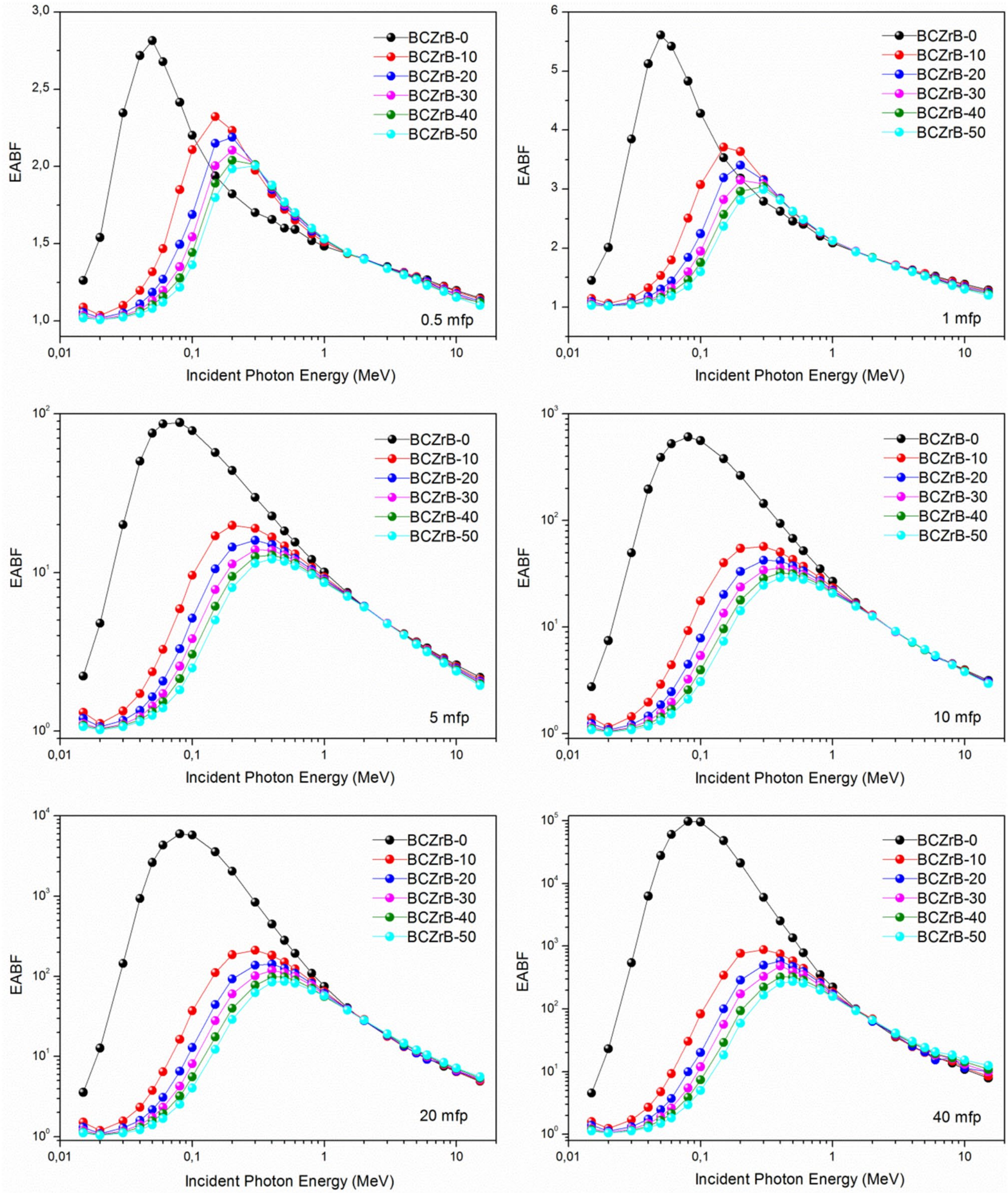

Fig. 9 *EABF* values of the ternary composites in the energy range from 0.015 MeV to 15 MeV at 0.5 *mfp*, 1 *mfp*, 5 *mfp*, 10 *mfp*, 20 *mfp* and 40 *mfp*

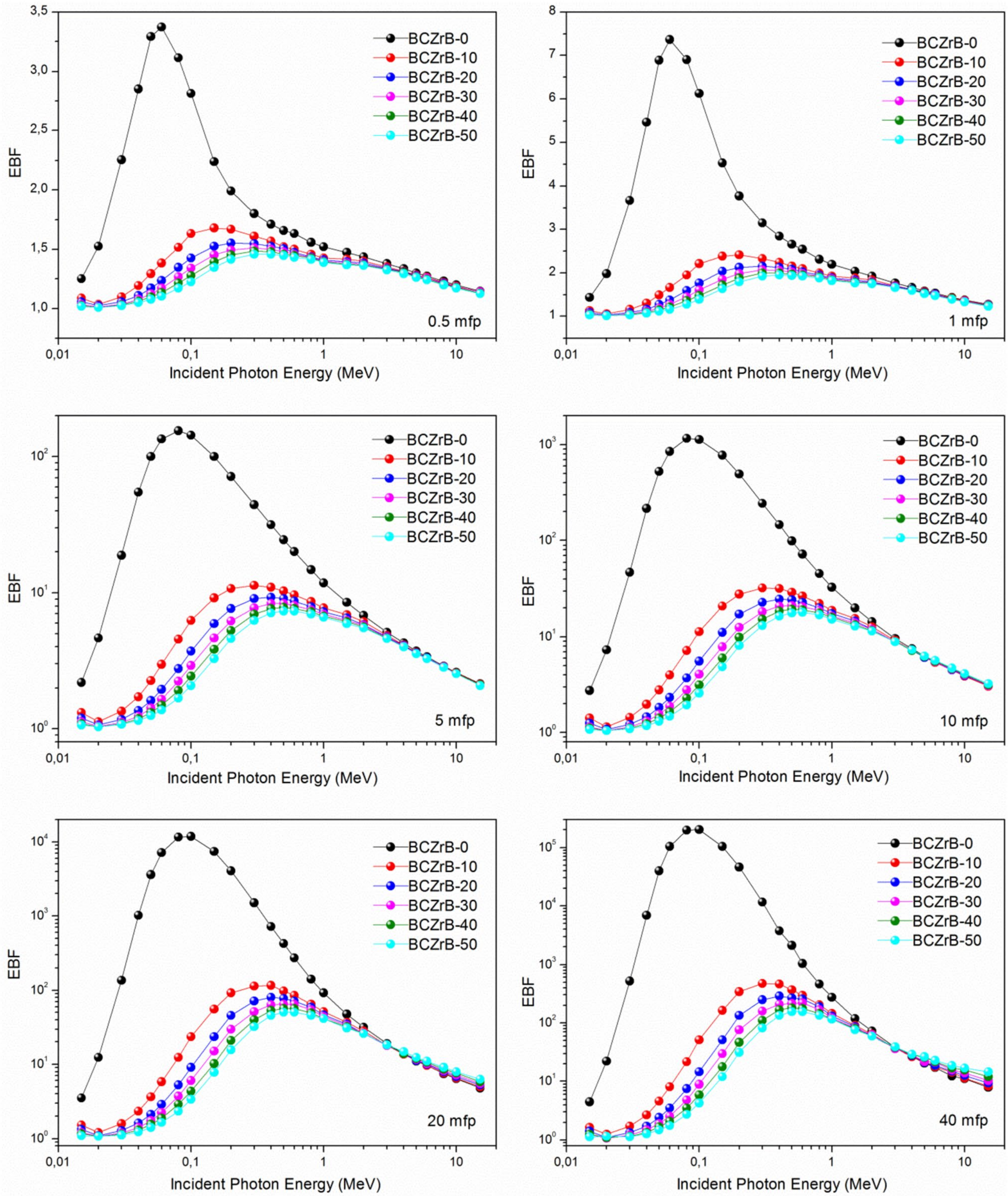

Fig. 10 *EABF* values of the ternary composites in the energy range from 0.015 MeV to 15 MeV at 0.5 *mfp*, 1 *mfp*, 5 *mfp*, 10 *mfp*, 20 *mfp* and 40 *mfp*

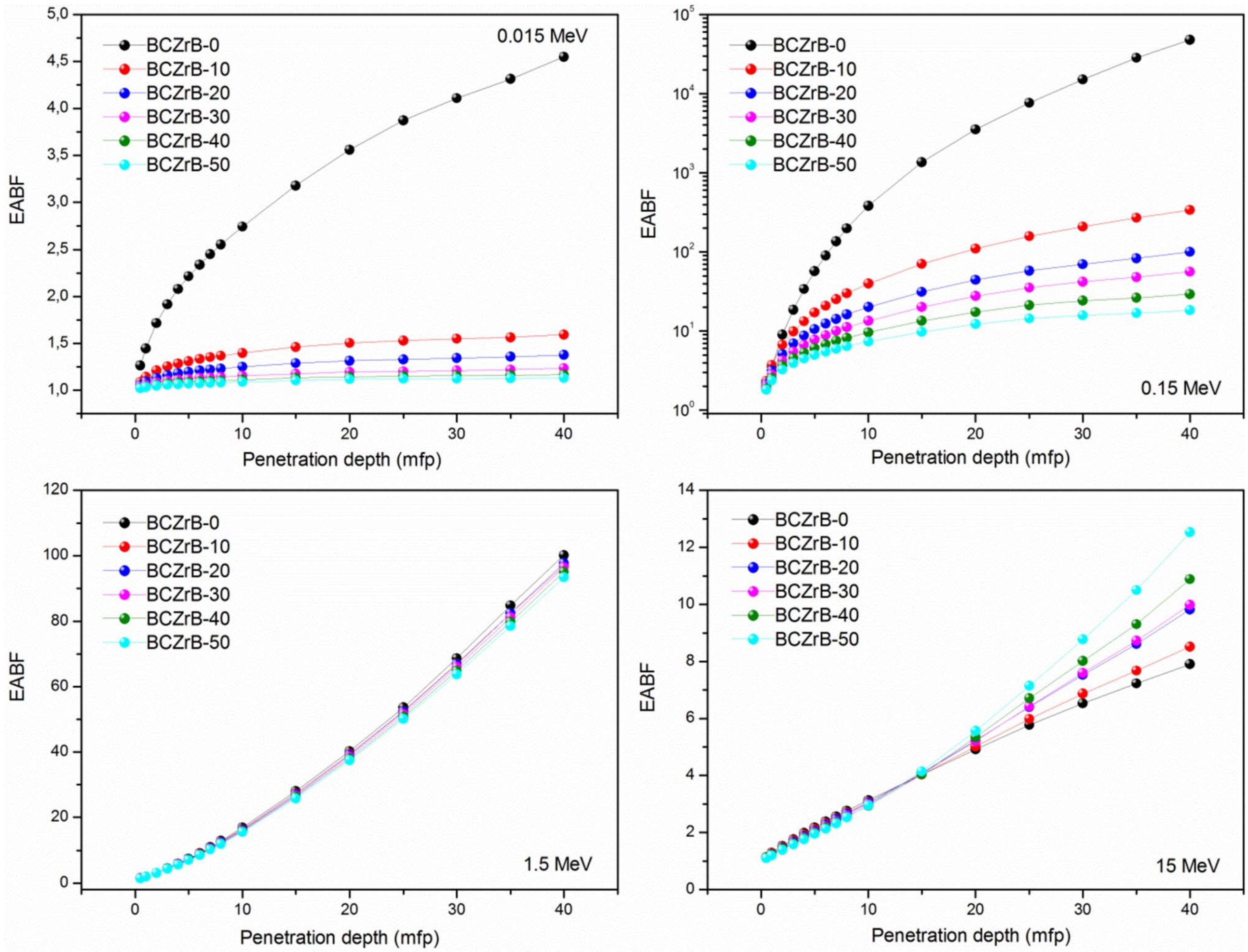

Fig. 11 *EABF* values of the ternary composites up to 40 *mfp* at 0.015, 0.15, 1.5, 15 MeV

$$W_i = (t_i)(\rho)_s \tag{20}$$

where W_i and $(\Sigma_R/\rho)_i$ are the partial density (g.cm^{-3}) and mass removal cross section (cm^2.g^{-1}) of the ith element, respectively. t_i and ρ_i are weight fraction of the ith constituent element in the material and the total density of the material, respectively.

4 Result and discussion

4.1 Results of *RPE*, *μ/ρ*, *μ*, *HVL*, *TVL* and *MFP*

Radiation protection efficiency (*RPE*) values were defined in the energy region 59.5 keV ≤ E ≤ 1332.5 keV with Eq. 2 for BCZrB-0, BCZrB-10, BCZrB-20, BCZrB-30, BCZrB-40 and BCZrB-50. Theoretical and simulation results as well as experimental results of *RPE* values for the composites under investigation are illustrated in Fig. 2. As seen from Fig. 2, the *RPE* values decrease exponentially in the low energy region. After that, this decreases linearly continuous more slightly in the energy region 276.4 keV ≤ E ≤ 1332.5 keV.

To determine the total mass attenuation coefficient, Eq. 3 was used for ternary composites. Experimental results for *μ/ρ* in the energy region 59.5 keV ≤ E ≤ 1332.5 keV are given in Table 2 and Fig. 3 along with WinXCOM, GEANT 4 and FLUKA. Also, experimental *μ* values for BCZrB-0, BCZrB-10, BCZrB-20, BCZrB-30, BCZrB-40 and BCZrB-50 are illustrated in Fig. 4. As seen from Table 2, Fig. 3 and 4, both total mass attenuation coefficients and linear attenuation coefficients for ternary composites increase proportionally to the filling ratio of boron. In addition, these values decrease non-linearly with increasing photon energy. Table 2 and Fig. 3 show that the difference between experimental and WinXCOM program, between experimental and GEANT 4 simulation codes and between experimental and FLUKA simulation codes of μ/ρ values are < 5.1%, < 6.5% and < 5.1%, respectively. The difference

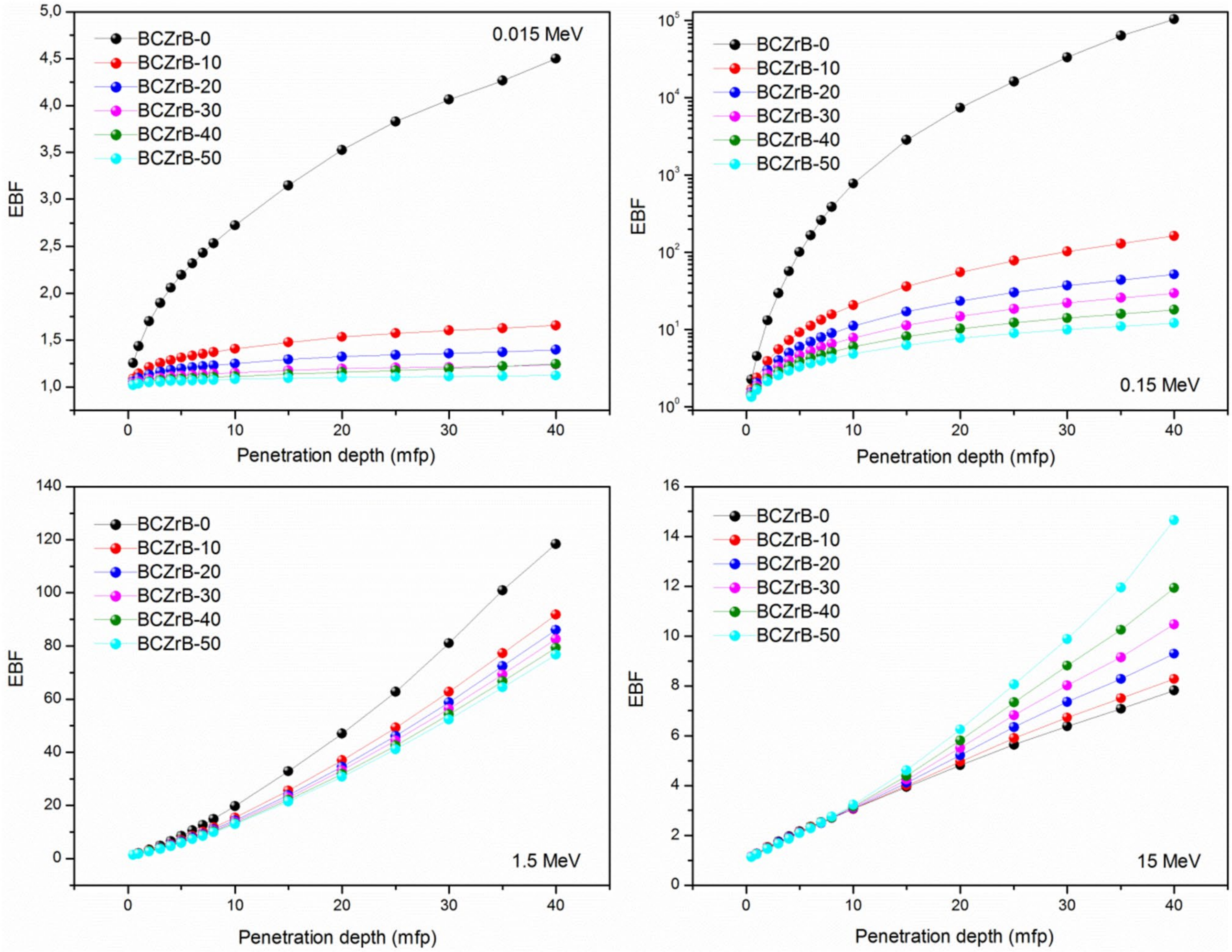

Fig. 12 *EABF* values of the ternary composites up to 40 *mfp* at 0.015, 0.15, 1.5, 15 MeV

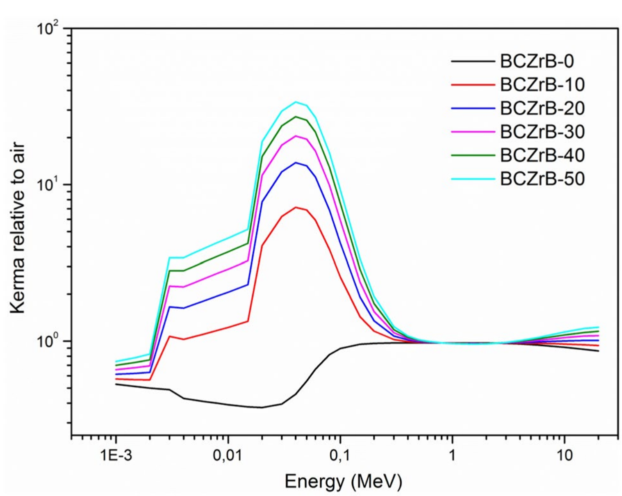

Fig. 13 Kerma relative to air values of the ternary composites in the energy region 0.001 MeV–20 MeV

between experimental and WinXCOM, GEANT 4 and FLUKA of the total mass attenuation coefficients may be due to the uncertainty of the photon intensities, mass per unit area of absorber samples and systematic errors in the experiment. So, it can be said that there is a good agreement between the experimental, WinXCOM, GEANT4 and FLUKA results with overall uncertainty. The experimental uncertainties were determined with Eq. 21 as follow [38];

$$\Delta\mu_m = \frac{1}{\rho x}\sqrt{\left(\frac{\Delta I}{I}\right)^2 + \left(\frac{\Delta I_0}{I_0}\right)^2 + ln\left(\frac{\Delta I}{I}\right)^2\left(\frac{\Delta \rho x}{\rho x}\right)^2} \quad (21)$$

where ρ and x are the density and thickness of the target, respectively. I_o and I are incident photons intensity and the transmitted photon intensity, respectively. ΔI_0 and ΔI are the uncertainties for the incident photons intensity (I_0) and transmitted photon intensity (I), respectively. The overall uncertainty in the total mass attenuation coefficient is approximately < ~5.5%. This uncertainty is attributed to the

Table 4 Effective removal cross sections for the ternary composites

Element	BCZrB-0 ($\rho = 1.8160$ g cm^{-3})		BCZrB-10 ($\rho = 1.8705$ g cm^{-3})		BCZrB-20 ($\rho = 1.9283$ g cm^{-3})		BCZrB-30 ($\rho = 1.9897$ g cm^{-3})		BCZrB-40 ($\rho = 2.0553$ g cm^{-3})		BCZrB-50 ($\rho = 2.1253$ g cm^{-3})	
	Partial density	Σ_R (cm^{-1})	Partial density	Σ_R (cm^{-1})	Partial density	Σ_R (cm^{-1})	Partial density	Σ_R (cm^{-1})	Partial density	Σ_R (cm^{-1})	Partial density	Σ_R (cm^{-1})
H	0.025273	0.015113	0.026030	0.015566	0.026835	0.016047	0.027690	0.016559	0.028602	0.017104	0.029577	0.017687
B	0.980335	0.056369	0.933471	0.053675	0.883710	0.050813	0.830776	0.047770	0.774354	0.044525	0.714089	0.041060
C	0.611665	0.030706	0.601957	0.030218	0.591649	0.029701	0.580683	0.029150	0.568995	0.028564	0.556511	0.027937
O	0.198674	0.008046	0.204630	0.008288	0.210954	0.008544	0.217681	0.008816	0.224851	0.009106	0.232510	0.009417
Co	0.000067	0.000001	0.000069	0.000001	0.000071	0.000001	0.000073	0.000001	0.000076	0.000001	0.000078	0.000002
Zr	–	–	0.104296	0.001627	0.215039	0.003355	0.332844	0.005192	0.458410	0.007151	0.592530	0.009243
Total	1.816014	0.110235	1.870453	0.109375	1.928257	0.108461	1.989747	0.107489	2.055289	0.106452	2.125295	0.105345

Table 5 Total macroscopic cross sections, mean free paths and number of transmitted neutrons of 10 mm thickness sample and 10^7 neutrons at 4.5 MeV for the ternary composites

Sample code	Total macroscopic cross section (cm^{-1})	Mean free path (mm)	Number of transmitted neutrons
BCZrB-0	2.0584	4.8581	8,435,561
BCZrB-10	2.0573	4.8607	8,444,792
BCZrB-20	2.0565	4.8626	8,456,008
BCZrB-30	2.0564	4.8629	8,464,973
BCZrB-40	2.0557	4.8645	8,475,630
BCZrB-50	2.0567	4.8621	8,488,265

uncertainties of the photon intensities ($< \sim 1.8\%$), mass per unit area of targets ($\leq 2.1\%$) and systematic errors ($\leq 2.3\%$). As seen from Table 2, Fig. 3 and 4, the results are in good agreement with each other. Also, present results indicated same performances with other studies [12, 17, 34].

In order to determine the *HVL*, *TVL* and *MFP* values for BCZrB-0, BCZrB-10, BCZrB-20, BCZrB-30, BCZrB-40 and BCZrB-50, Eq. 6, 7 and 8 are used, respectively. Experimental *HVL* values in the energy range from 59.5 keV to 1332.5 keV for ternary composites were showed in Fig. 5. Also, both experimental *TVL* values and experimental *MFP* values of the ternary composites were illustrated in Fig. 6. Figure 5 and 6 show that the *HVL*, *TVL* and *MFP* values for ternary composites increase exponentially with increasing photon energy in the energy region 59.5 keV $\leq$ E $\leq$ 1332.5 keV. While BCZrB-0 ternary composite receive the biggest *HVL*, *TVL* and *MFP* values at all measured energy points, BCZrB-50 ternary composite take the smallest values at all measured energy points.

4.2 Results of Z_{eff} and N_{eff}

Equation 9 and 10 used for effective atomic number and effective electron density values for ternary composites. Experimental results for Z_{eff} in the energy range from 59.5 keV to 1332.5 keV were listed in Table 3 along with WinXCOM, GEANT 4 and FLUKA and illustrated in Fig. 7. Figure 8 shows the experimental N_{eff} values for BCZrB-0, BCZrB-10, BCZrB-20, BCZrB-30, BCZrB-40 and BCZrB-50. As seen from Table 3 and Fig. 7, the difference between experimental and WinXCOM program, between experimental and GEANT 4 simulation codes and between experimental and FLUKA simulation codes of Z_{eff} values are $< 5.1\%$, $< 6.5\%$ and $< 5\%$, respectively. Table 3, Fig. 7 and 8 show that Z_{eff} and N_{eff} values of the BCZrB-0 are nearly constant. With the increasing contribution of the baron, the changing values in the BCZrB-10, BCZrB-20, BCZrB-30, BCZrB-40 and BCZrB-50 are seen clearly from the Table 3, Fig. 7 and 8. Z_{eff} and N_{eff} values decrease exponentially in

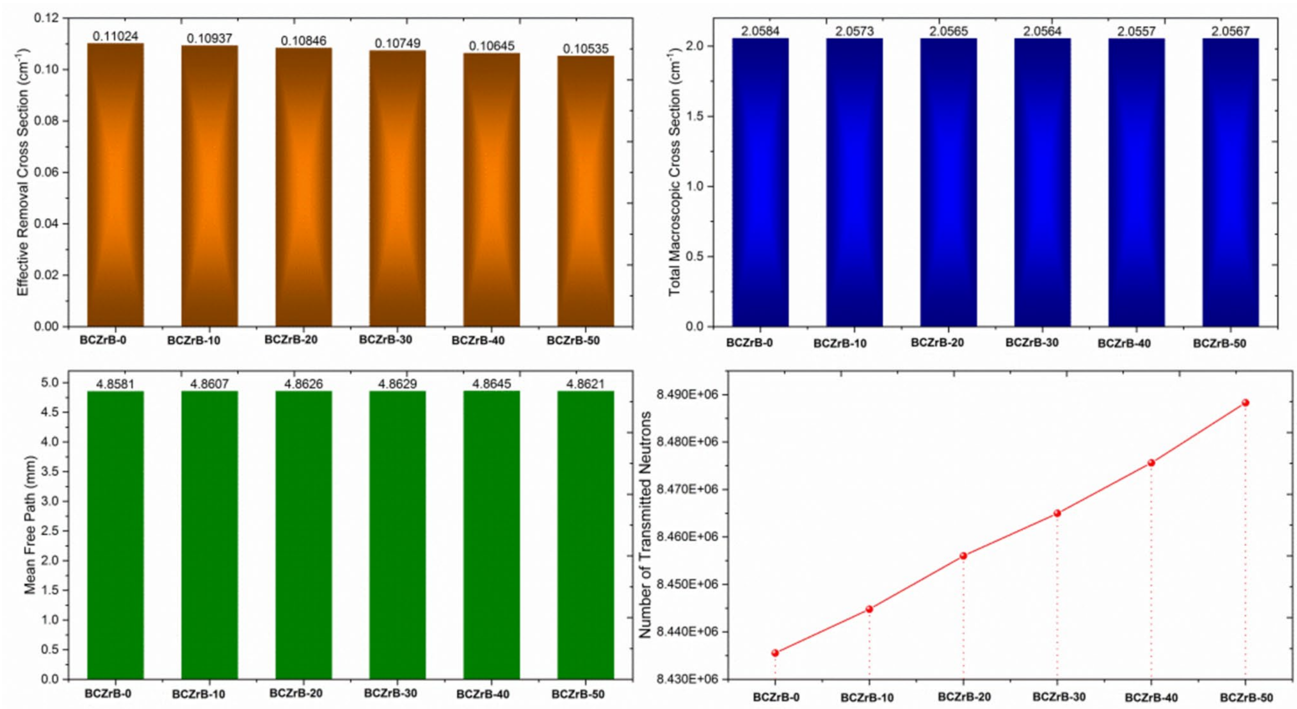

Fig. 14 Effective removal cross sections, total macroscopic cross sections, mean free paths and number of transmitted neutrons of the ternary composites

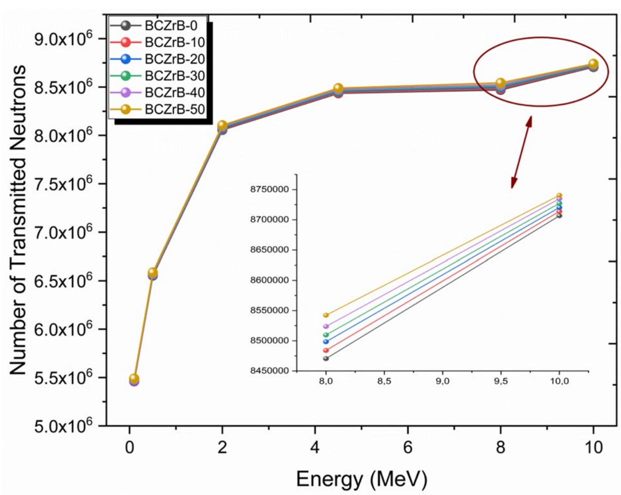

Fig. 15 Number of transmitted neutron values of the ternary composites versus photon energy

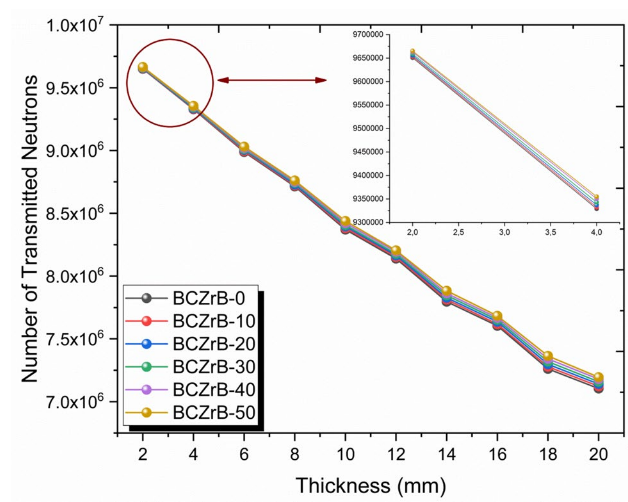

Fig. 16 Number of transmitted neutron values of the ternary composites versus thickness

the low energy region after that a sharp decrease in the rate of decrease of values except for BCZrB-0 is observed from Table 3, Fig. 7 and 8. Finally, Z_{eff} and N_{eff} values become almost constant in the high energy region. This result shows that different interactions predominate in different energy regions. Also, present results indicated same performances with other studies [3, 19].

4.3 Results of build-up factors

Using G-P fitting parameters calculated from ANSI/ANS-6.4.3 [35], *EABF* and *EBF* were theoretically calculated from Eq. 13–15 in the energy range from 0.015 MeV to 15 MeV at different penetration depths. Graph of energy absorption build-up factors (*EABF*) versus energy in energy region 0.015 MeV ≤ E ≤ 15 MeV at dissimilar penetration depth such as 0.5 *mfp*, 1 *mfp*, 5 *mfp*, 10 *mfp*, 20 *mfp* and 40 *mfp* is pictured in Fig. 9 for BCZrB-0, BCZrB-10, BCZrB-20, BCZrB-30, BCZrB-40 and BCZrB-50. Also, Fig. 10 shows the exposure build-up factors (*EBF*) versus energy in the energy range from 0.015 MeV to 15 MeV at 0.5 *mfp*, 1 *mfp*, 5 *mfp*, 10 *mfp*, 20 *mfp* and 40 *mfp* penetration depths for ternary composites. As seen from Fig. 9 and 10, *EABF* and *EBF* values increase non linearly with increasing energy in the low energy region all penetration depths. After that the values sharply (around 0.08 MeV to 1 MeV) and after slowly (around 1 MeV to 15 MeV) decrease with increasing photon energy in the medium and high energy region all penetration depths, respectively. While BCZrB-0 is generally take the highest values in the low and intermediate energy regions, BCZrB-50 generally take the highest values in the high energy region with increasing penetration depths. Graph of energy absorption build-up factors (*EABF*) versus penetration depth (*mfp*) at 0.015 MeV, 0.15 MeV, 1.5 MeV and 15 MeV is illustrated in Fig. 11. Also, Fig. 12 shows the exposure build-up factors (*EBF*) versus penetration depth (*mfp*) at the 0.015 MeV, 0.15 MeV, 1.5 MeV and 15 MeV. It is obviously seen from Fig. 11 and 12, *EABF* and *EBF* values increase exponentially with increasing penetration depth. While *EABF* and *EBF* values at 0.015 MeV could be ranked as: BCZrB-0 > BCZrB-10 > BCZrB-20 > BCZrB-30 > BCZrB-40 > BCZrB-50, *EABF* and *EBF* values take the reverse trend at 15 MeV like BCZrB-50 > BCZrB-40 > BCZrB-30 > BCZrB-20 > BCZrB-10 > BCZrB-0. It is obviously seen from Fig. 11 and 12, BCZrB-50 took the biggest value with increasing energy.

4.4 Results of kerma relative to air and effective removal cross-section.

Figure 13 shows the kerma relative to air values versus photon energy in the energy region 1 keV ≤ E ≤ 20 MeV. Figure 13 show that values increase non-linearly with increasing photon energy up to ~ 350 keV except for BCZrB-0. While BCZrB-0 values increase with increasing in the intermediate energy region, the values of the other ternary composites are tend to reverse. Finally, the values of the all ternary composites show slightly increase or decrease non-linearly around high energy region. The results support each other.

Effective removal cross sections (Σ_R) are listed with partial density for ternary composites in Table 4. Also, Table 5 shows the total macroscopic cross sections, mean free paths and number of transmitted neutrons of 10 mm thickness sample and 10^7 neutrons at 4.5 MeV for the ternary composites. Effective removal cross sections, total macroscopic cross sections, mean free paths and number of transmitted neutrons for BCZrB-0, BCZrB-10, BCZrB-20, BCZrB-30, BCZrB-40, BCZrB-50 are illustrated in Fig. 14. Number of transmitted neutron values versus photon energy for ternary composites are imagined in Fig. 15 with GEANT 4 simulation package. Also, number of transmitted neutron values versus thickness for ternary composites are illustrated in Fig. 16 with GEANT 4 simulation package. As seen from Table 4 and Fig. 14, effective removal cross sections decrease with increasing filled boron ratio. It is obviously seen from Table 5 and Fig. 14, total macroscopic cross section values are the range from 2.0557 cm^{-1} to 2.0584 cm^{-1} and also, mean free path are the range from 4.8581 mm to 4.8645 mm. As seen from Table 5 and Fig. 14, number of transmitted neutron values are 8,435,561 for BCZrB-0, 8,444,792 for BCZrB-10, 8,456,008 for BCZrB-20, 8,464,973 for BCZrB-30, 8,475,630 for BCZrB-40 and 8,488,265 for BCZrB-50 and could be ranked as: BCZrB-0 < BCZrB-10 < BCZrB-20 < BCZrB-30 < BCZrB-40 < BCZrB-50. It is obviously seen from Fig. 15, number of transmitted neutron values increase exponentially with increasing energy. Finally, according to Fig. 16, number of transmitted neutron values decrease linearly with increasing thickness. BCZrB-0 has the best neutron attenuation values in the studied composites.

5 Conclusion

First of all in the study, *RPE*, μ/ρ, μ, *HVL*, *TVL*, *MFP*, Z_{eff} and N_{eff} values were investigated for BCZrB-0, BCZrB-10, BCZrB-20, BCZrB-30, BCZrB-40 and BCZrB-50. WinXCOM, GEANT4 simulation code and FLUKA simulation code were used in addition to experimental investigation to determine the absorption parameters in the energy region 59.5 keV ≤ E ≤ 1332.5 keV. Secondly, *EABF* and *EBF* values for ternary composites in the energy region 0.015 MeV ≤ E ≤ 15 MeV were calculated with G-P fitting method. Thirdly, kerma relative to air values for ternary composites were computed in the energy range from 0.001 MeV to 20 MeV. Finally, effective removal cross section, total macroscopic cross section and number of transmitted neutron values were determined for ternary composites. In the study, results obtained using different techniques were compared with each other. As seen from tables and figures, all of the results are compatible with each other. μ/ρ values found to be 0.1707—0.0524 cm^2g^{-1}, 0.3793—0.0527 cm^2g^{-1}, 0.5794—0.0531 cm^2g^{-1}, 0.7838—0.0525 cm^2g^{-1}, 0.9895—0.0530 cm^2g^{-1}, 1.1941—0.0526 cm^2g^{-1} for BCZrB-0, BCZrB-10, BCZrB-20, BCZrB-30, BCZrB-40 and BCZrB-50, respectively. Also, Σ_R values found to be in the range from 0.105345—0.110235 cm^{-1} for ternary composites. Considering the all results from experimental, WinXCOM, GEANT4 and FLUKA simulation codes, it can be concluded that WinXCOM, GEANT4 and FLUKA simulation codes are quite suitable for calculating the radiation interaction parameters of studied composites. Also, BCZrB-50 generally take the highest *RPE*, μ/ρ, μ, Z_{eff}, N_{eff}, kerma relative to air, number of transmitted neutron values and the lowest *HVL*, *TVL*, *MFP*, Σ_R, *EABF* and *EBF* (except for high *mfp* and energy) values. According to the results obtained from tables and figures, BCZrB-50 is the best gamma or X-ray radiation absorber in the studied composites and also, BCZrB-0 is the best neutron absorber in the studied composites. These values show that gamma radiation attenuation capacity increases with increasing amount of the zirconium boride. The present results may contribute to numerous application areas related to radiation research.

Authors contribution M. F. Turhan: Conceptualization, Validation, Formal analysis, Investigation, Methodology, Writing—Original Draft, Writing—Review & Editing, Visualization, Supervision. A.Tursucu: Conceptualization, Validation, Formal analysis, Methodology, Data Curation, Writing—Original Draft, Writing—Review & Editing, Visualization. H.Oğul: Validation, Formal analysis, Methodology, Methodology, Data Curation, Writing—Original Draft, Writing—Review & Editing, Visualization. M.R.Kaçal: Validation, Formal analysis, Methodology, Writing—Original Draft, Visualization. H.Polat: Investigation, Writing—Original Draft, Resources, Visualization. E. Colak: Writing—Original Draft, Data Curation, Resources. S.Yurtcan: Writing—Original Draft, Data Curation, Resources. F. Akman: Data Curation, Writing—Original Draft, Writing—Review & Editing, Supervision.

Data availability The data that has been used is confidential.

Declarations

Conflict of interest No potential conflict of interest was reported by the authors.

References

1. S. Banerjee, S. Basu, A.D. Baheti, S. Kulkarni, V. Rangarajan, P. Nayak, V. Murthy, A. Kumar, S.G. Laskar, J.P. Agarwal, S. Gupta, R.A. Badwe, Curr. Sci. **123**(3), 388–395 (2022)
2. D. Schmeda-Lopez, T.B. McConnaughy, E.W. McFarland, Energy **162**, 491–504 (2018)
3. F. Akman, H. Ogul, I. Ozkan, M.R. Kaçal, O. Agar, H. Polat, K. Dilsiz, Nucl. Eng. Technol. **54**, 283–292 (2022)
4. B. Ranković, V. Gajić, S. Mašić, V. Pavićević, I. Vujčić, Appl. Radiat. Isot. **192**, 110602 (2023)
5. B.T. Sendja, N.A.M. Castillo, R.L. Portales, S.T. Kouonang, G.J.L. Delgado, C.C. Alvarez, L. Olivi, Physica B Condens. Matter **617**, 413128 (2021)
6. M.F. Turhan, F. Akman, H. Polat, M.R. Kaçal, İ Demirkol, Prog. Nuclear Energy **129**, 103504 (2020)
7. M.R. Kaçal, H. Polat, M. Oltulu, F. Akman, O. Ağar, H.O. Tekin, Appl. Phys. A **126**, 205 (2020)
8. F. Akman, H. Oğul, M.R. Kaçal, H. Polat, K. Dilsiz, M.F. Turhan, Appl. Phys. A **126**, 301 (2020)
9. R. Mirji, B. Lobo, J. Radioanal. Nucl. Chem. **324**, 7–19 (2020)
10. E. Kalkornsurapranee, S. Kothan, S. Intom, J. Johns, S. Kaewjaeng, C. Kedkaew, W. Chaiphaksa, T. Sareein, J. Kaewkhao, Radiat. Phys. Chem. **179**, 109261 (2021)
11. N.A. Kawady, M. Elkattan, M. Salah, A.A. Galhoum, J. Matter. Sci. **57**, 11046–11061 (2022)
12. F. Akman, H. Ozdogan, O. Kilicoglu, H. Ogul, O. Agar, M.R. Kacal, H. Polat, A. Tursucu, Radiat. Phys. Chem. **212**, 111120 (2023)
13. M. Irfan, M. Aslam, Z.A. Raza, Polym. Bull. **80**, 791–807 (2023)
14. S.M. Kassem, M.I.A. Abdel Maksoud, M.M. Ghobashy, A.M. El Sayed, S. Ebraheem, A.I. Helal, Y.Y. Ebaid, Radiat. Phys. Chem. 209, 110953 (2023)
15. M. Dong, S. Zhou, H. Yang, X. Xue, Nucl. Eng. Technol. **55**, 2613–2620 (2023)
16. R.B. Malidarre, I. Akkurt, M.Y. Imamoglu, J. Aust. Ceram. Soc. **59**, 369–377 (2023)
17. A.H. Alsaab, S. Zeghib, J. Radiat. Res. Appl. Sci. **16**, 100708 (2023)
18. A.M. El-Khatib, K. Zard, M.I. Abbas, M.M. Gouda, Sci. Rep. **14**, 1578 (2024)
19. G. ALMisned, F. Akman, W.S. AbuShanab, H.O. Tekin, M.R. Kaçal, S.A.M. Issa, H. Polat, M. Oltulu, A. Ene, H.M.H. Zakaly, Polymers 13, 3157 (2021)
20. H.H. Sarteshnizi, M. Eshghi, Radiat. Detect. Technol Methods **8**, 1217–1228 (2024)
21. X. Zhang, Y. Zhao, M. Zhang, H. Liu, Y. Yao, T. Cheng, H. Chen, J. Phys. Condens. Matter **29**, 455401 (2017)
22. R. Matschat, A. Dette, S. Richter, S. Recknagel, P. Barth, J. Am. Ceram. Soc. **94**(11), 4009–4016 (2011)
23. K.K. Yadav, S.K. Guchhait, C.M. Sunaina, Ankush, Hussain, A.K. Ganguli, M. Jha, J. Solid State Electrochem. 23, 3243–3253 (2019)
24. N. Gupta, B. Basu, *Intermetallic Matrix Composites Properties and Applications*, pp. 243–302 (2018)
25. H.T. Hattori, S. Member, A. Haque, B.C. Olbricht, Z. Li, IEEE Photon. Technol. Lett. **30**(1), 11–14 (2018)
26. F. Akman, M.F. Turhan, H. Oğul, A. Turşucu, T. Erdoğan, M.R. Kaçal, H. Polat, Radiat. Phys. Chem. **226**, 112326 (2025)
27. L. Gerward, N. Guilbert, K.B. Jensen, H. Levring, Radiat. Phys. Chem. **71**, 653–654 (2004)
28. S. Agostinelli, J. Allison, K. Amako, J. Apostolakis, H. Araujo, P. Arce et al., Nucl. Instrum. Meth. A **506**, 250–303 (2003)
29. T.T. Böhlen, F. Cerutti, M.P.W. Chin, A. Fassò, A. Ferrari, P.G. Ortega, A. Mairani, P.R. Sala, G. Smirnov, V. Vlachoudis, Nucl. Data Sheets **120**, 211–214 (2014)
30. İ Erkoyuncu, F. Akman, H. Ogul, M.R. Kaçal, H. Polat, İ Demirkol, K. Dilsiz, B. Ertuğral, Appl. Radiat. Isot. **196**, 110789 (2023)
31. H. Oğul, O. Agar, F. Bulut, M.R. Kaçal, K. Dilsiz, H. Polat, F. Akman, Appl. Radiat. Isot. **194**, 110731 (2023)
32. B. Gultekin, H. Ogul, Radiochim. Acta **111**(2), 137–145 (2023)
33. H. Oğul, H. Polat, F. Akman, M.R. Kaçal, K. Dilsiz, F. Bulut, O. Agar, Radiat. Phys. Chem. **201**, 110474 (2022)
34. M.F. Turhan, F. Akman, A. Taşer, K. Dilsiz, H. Oğul, M.R. Kaçal, O. Agar, Prog. Nucl. Energy **143**, 104036 (2022)
35. ANSI/ANS-6.4.3, *Gamma Ray Attenuation Coefficient and Buildup Factors for Engineering Materials* (American Nuclear Society, La Grange Park, IL, USA, 1991)
36. M.F. Kaplan, *Concrete Radiation Shielding* (John Wiley & Sons, New York, USA, 1989)

37. J. Wood, *Computational Methods in Reactor Shielding* (Pergamon Press Inc, New York, USA, 1982)
38. F. Ozel, F. Akman, M.R. Kaçal, A. Ozen, H. Arslan, H. Polat, S. Yurtcan, O. Agar, J. Phys. Chem. Solids **158**, 110238 (2021)